Monitoring Human-Induced Surface Water Disturbance Around Taihu Lake Since 1984 by Time Series Landsat Images

Yaping Meng, Peijun Du, *Senior Member, IEEE*, Xin Wang, Xuyu Bai, and Shanchuan Guo

***Abstract*—Good knowledge of inland water dynamics is of great significance for water management, preserving ecological balance and supporting industrial and agricultural development. However, the existing water cover products and water extraction methods cannot meet the present needs of monitoring water distribution and dynamic changes accurately and timely, particularly in the areas frequently disturbed by human activities, such as the Taihu Lake region. This article proposed an expert knowledge system to detect annual stable water and separate aquaculture water from natural water, and a frequency-based approach is used to generate stable water map within a year. All available Landsat Level-2 images were used to generate annual 30-m resolution stable water products from 1984 to 2018, and analyze the historical spatial–temporal changes of the water body in the Taihu Lake region. Furthermore, we related each important graph change with a reality event at that time. The results suggest that human activities have an obviously stronger influence on surface water than climate fluctuations in the Taihu Lake region, and confirm the effectiveness of ecological protection policy in maintaining the stability of the total amount of natural water in the past few decades. The spatial–temporal disturbance of aquaculture also provided another perspective and a reliable evidence of previous studies on the influence of human activities on the eutrophication process of Taihu Lake.**

***Index Terms*—Aquaculture recognition, inland water extraction, Landsat images.**

I. Introduction

INLAND surface water, mainly including lakes, reservoirs, rivers, and other elements, is essential to the terrestrial ecosystem where many organisms inhabit and the social and economic development [1], [2]. In recent years, climate change and human activities, such as urban expansion, reclamation, and eutrophication, have been causing lake shrinkage and water quality degradation, these problems attracted wide attention. Moreover, frequent cyanobacteria outbreaks also posed a great threat to the ecological environment [3]. These problems are particularly prominent in the Taihu Lake Basin, one of the most water-rich regions in China, with high degree of urbanization and dense population. Thus, the local water resources cannot fully meet the huge demand of industrial, agricultural, and domestic water use. In addition, the diverse and frequent human activities have been causing water loss and water pollution for decades, further exacerbating this problem. In view of the tradeoff between development and environment, there is a need to acquire the accurate information on water distribution and implement dynamic monitoring of water body for matching the perspective of ecological safety and sustainable development. Particularly, spatial–temporal change analysis of surface water that depicts the characteristics of water disturbance and helps to reveal the causes of water reduction and pollution.

In previous studies, some well-known land cover products with spatial resolution finer than 500 m (FROM-GLC10, GlobalLand30, ESA-CCI, GLCNMO, and GLS) [4]–[9] and global water mask datasets (G3WBM, SWBD, GLCF MODIS, GLCF GIW, GLOWABO, GIEMS-D15, GSW, and Global WaterPack) [10]–[16] have been produced, which can help us understand the distribution and change of water. FROM-GLC10, GlobeLand30, and GLS, with high classification accuracy and high spatial resolution [5], [6], [8] can assist the study of the distribution of water body on a watershed scale but cannot apply to the monitoring of rapid changes in surface water bodies over the past few decades, in other words, the updated global LULC products can only reflect land cover situations in 2012 (GlobeLand30) and 2017 (FROM-GLC10). In terms of thematic water data, G3WBM and GSW are two widely used datasets, of which G3WBM is stable surface water derived from five periods of GLS dataset from 1975 to 2010, with the highest classification accuracy compared to other thematic data products [13]. GSW provides a global water cover map from 1984 to 2015 with the highest spatial resolution, the largest coverage area and the longest time span so far [15]. However, this dataset does not perform well in many shallow lakes and artificial water body, and omissions and mismatches often occur in GSW due to the coverage of aquatic plants. This problem also exists in many other water products at present.

A large number of classifiers have been used to remote sensing image classification and target recognition, in which random forest and SVM mostly have a better performance in terms of accuracy and generalization capacity [17]–[21]. However, these methods usually draw accurate land cover maps for small areas

Manuscript received December 1, 2019; revised April 17, 2020 and June 18, 2020; accepted June 21, 2020. Date of publication June 26, 2020; date of current version July 8, 2020. This work was supported by the Natural Science Foundation of China under Grant 41631176. *(Corresponding author: Peijun Du.)*

The authors are with the Key Laboratory for Land Satellite Remote Sensing Applications of Ministry of Natural Resources, the School of Geography and Ocean Science, and the Jiangsu Center for Collaborative Innovation in Geographical Information Resource Development and Application, Nanjing University, Nanjing 210023, China (e-mail: ypmengnju@126.com; dupjrs@126.com; wangxrs@126.com; baixy26@163.com; gsc@smail.nju.edu.cn).

Digital Object Identifier 10.1109/JSTARS.2020.3005135

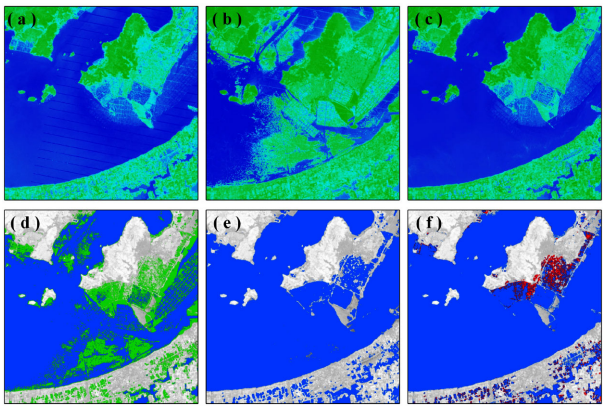

Fig. 1. Commission error in previous water products. (a) MNDWI in winter 2012 (High value in blue, low value in green). (b) MNDWI in summer 2013. (c) MNDWI in winter. (d) GSW water mask of 2013 (Permanent water marked as blue, seasonal water marked as green). (e) Water cover in 2017 from FROMGLC10. (f) Commission error in FROMGLC10 (marked as red).

at specific times, and the characteristic differences within the categories become more pronounced with the expansion of time scales and spatial ranges, and high cost of selecting training samples limits the use of classification method to analyze a broader range of spatio–temporal variability and trends [22]. In addition to the expensive methods mentioned earlier, lots of low-cost methods for detecting water from optical remote sensing images were proposed. Water indices were widely used because they can enhance the difference between water body and others, such as the wetness component of TC transformation [23], NDWI [24], MNDWI [25], AWEI [26], and WI2015 [27]. In practical applications, MNDWI performs better than other indices, with high contrast between water body and vegetation, soil and built-up background, and has a low sensitivity to the concentration of sediments and other optically active components in water. Furthermore, the aforementioned indices can be integrated to enhance the performance of water extraction [28], [29]. In particular, the introduction of NDVI has a better performance in automated extraction method of rivers and other easily omitted water body [30]. In addition, DEM is often used as an auxiliary data to eliminate the confusion of mountain shadows and water bodies [31], [32].

Inland aquaculture is a special type of artificial water. Besides exchanging material with natural water and causing pollution, aquaculture not only changes the morphological characteristics of nonfarmed water and wetland, but also changes the interactions with ecological environment. Besides, it should be noticed that aquaculture has been developed rapidly and accounted for a considerable fraction of all inland water. However, in previous water products, aquaculture and natural water bodies were not distinguished, as shown in Fig. 1, making it difficult to assess the disturbance of surface water [6], [8], [15]. It is necessary but difficult to separate aquaculture from natural water because of their confusing appearance and phenological characteristics. Existing methods often introduce geometric and texture characteristics into a classifier to reclassify water masks as aquaculture and natural water [33], [34]. However, these methods are limited by the huge computational and complex parameter selection, making it difficult to monitor the dynamics of aquaculture using time series remote sensing images.

In addition to extraction and classification methods, some other issues should be considered. First, the distribution of aquatic plants in natural and aquaculture water has spatial and temporal variability. Aquatic plants are often the negative factors in extracting water bodies [35],[36], whereas positive factors in water reclassification, which makes it difficult to achieve this goal, by using remote sensing imagery acquired just in one season. The cloud and shadow coverage is an inevitable obstacle in mapping surface water as it causes partial or all of the valid observations to be lost on most images, which is another reason why the methods of mapping water with a single date image may lead to severe omission and commission error [36]. The frequency-based method, overcoming the problem of phonological changes and observations missing, can effectively identify and reclassify surface water [37].

Monitoring the spatial–temporal change in surface water is another important element. Unlike the slow changes in water body caused by climate change, water changes caused by human activities, such as urban expansion, reclamation, and aquaculture, occur at a high frequency. Knowing the exact time and location of historical changes in water body is vital for understanding human-earth relations, tracking the evolution process, and supporting water resource management. Continuous change detection is an effective way to study the temporal and spatial changes of land cover by generating change time raster to record the timing and location of changes simultaneously [38],[39].

In conclusion, both the released products and methods proposed by previous studies could not satisfy the current requirements of time series monitoring of water surface, causing the limitation in understanding the dynamics of Taihu Lake. In this study, time series Landsat TM/ETM+/OLI images are used to study spatial–temporal dynamics of surface water around the Taihu Lake from 1985 to 2018. The specific objectives are to develop an efficient water extraction algorithm to generate annual map of natural water and aquaculture water, and to improve the knowledge of spatial–temporal changes of water around the Taihu Lake.

II. Materials

A. Study Area

The Taihu Lake Basin is located in the eastern part of China, as shown in Fig. 2. The west of the basin is mountainous and hilly area, and the middle and east are plains and depressions. Such area is connected through dense water network and flat channel. All lakes in Taihu Lake Basin are shallow lakes, with the average water depth of less than 2 m and maximum water depth of less than 4 m. Taihu Lake Basin is in a subtropical monsoon climate, mild and rainy in summer, cold and dry in winter. The average annual temperature is 16–18 °C, and the annual precipitation is 1100–1150 mm. The average rainfall in flood season (including rainy season from May to July, and typhoon season in August and September) accounting for 60.4% of annual precipitation. With annual spring rain increasing, the water level rises to the highest water level (July and August). The water level begins to decline after September, and the lowest level occurs in December.

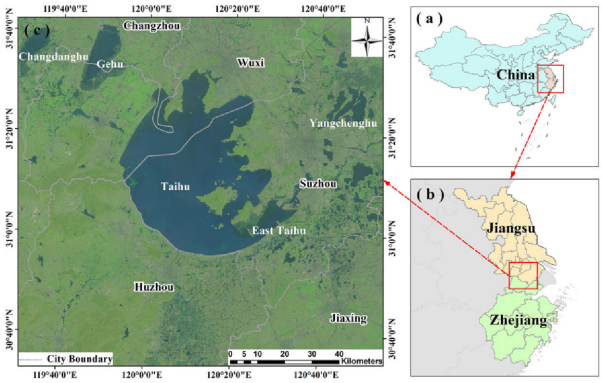

Fig. 2. Location of study area. (a) The location of Jiangsu and Zhejiang Province in China, the red rectangle indicates the range of these two provinces. (b) The location of the study area in Jiangsu and Zhejiang Province, the red rectangle indicates the range of the study area. (c) True color composite image (R, G, B = band 4, 3, 2) from Landsat-8 Operational Land Image (OLI) of the study area, acquired on 28th April 2018.

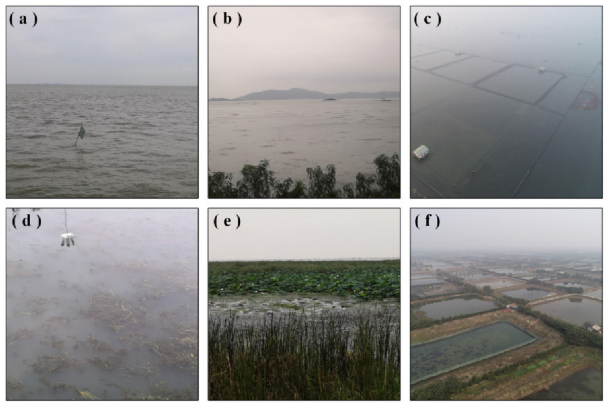

Fig. 3. Typical water types and their sampled images in the study area. (a) Open water body. (b) Natural water in the summer. (c) Aquatic-breeding water in the winter. (d) Pond farming in the summer. (e) Natural water covered by dense aquatic plants in summer. (f) Pond framing in the winter.

The research area is the central area of Taihu Lake Basin and an essential part of the Yangtze River Delta urban agglomeration, including southern Jiangsu province and northern Zhejiang province. It is an important aquaculture and agricultural area, with more than 11 600 km^2 arable land. The region has a high degree of urbanization, rapidly growing population, and fast industrial development, which has very high demands for water resources. The contradictions among urbanization development, human living, water resources, and the environment are quite strong in this area.

B. Data

Landsat Surface Reflectance Level-2 science products, deriving from Landsat Ecosystem Disturbance Adaptive Processing System, are used to support land surface change studies. Top of atmosphere reflectance and Pixel Quality Assessment band (pixel_qa) are used in this research.

All available Surface Reflectance Level-2 products at 30-m spatial resolution captured by Landsat 4, 5, 7, and 8 for Worldwide Reference System Path 119 and Row 38 and 39 were used. A total of 1276 Landsat-TM images, 767 Landsat-ETM+ images, and 252 Landsat-OLI images between 1984 and 2018 were used. Landsat 7 SLC-off data are not gap-filled in Surface Reflectance production, and about 25% information of each image is missing, these gaps were set to null values and masked off during further processing.

Surface reflectance products were used to derive several spectral indices related to water extraction. Modified Normalized Difference Water Index (MNDWI) and Normalized Difference Vegetation Index (NDVI) are used to extract water body, and cloud mask derived from pixel_qa data is used to correct miscalculation of water body [40].

MNDWI is calculated as

$$\text{MNDWI} = \frac{(\rho_G - \rho_{\text{MIR}})}{(\rho_G + \rho_{\text{MIR}})} \tag{1}$$

where ρ_G and ρ_{MIR} are reflectance in green spectra and mid infrared (MIR), respectively.

NDVI is calculated as

$$\text{NDVI} = \frac{(\rho_{\text{NIR}} - \rho_R)}{(\rho_{\text{NIR}} + \rho_R)} \tag{2}$$

where ρ_{NIR} and ρ_R are reflectance in near infrared (NIR) and red spectra, respectively.

The cloud mask was generated by using cloud indicators in pixel_qa data, only high confidence cloud was marked, for it is easy to confuse the water body with the medium- and low-confidence clouds in the CFmask algorithm, which could result in water omission. Images with a cloud coverage more than 80% were removed because there is too much interference information in these images.

The 30-m resolution ASTER Global Digital Elevation Model (GDEM) v2.0 dataset [4] downloaded from[1] was used as an important auxiliary data. The topographic slope is derived from GDEM to mask the mountain shadow off and the area with slope larger than 10° is considered to be nonwater areas.

III. Method

Instantaneous state recognition is the key to extract surface water from remote sensing images. Based on the spectral characteristics of several representative features of shallow lakes (see Fig. 3), a new method is proposed to extract the aquatic plants cover layer, and open water is merged with it to generate the instantaneous state mask. A frequency-based method that takes the phonological changes of ground targets into account is used to filter wrong classification objects, such as urban buildings, rice fields, and seasonal snowfall, in order to generate stable annual water coverage products. Fig. 4 shows the workflow of the proposed method.

A. Individual Water Extent

MNDWI was used to extract surface water, and an unsharp masking method was used to avoid narrow rivers and tiny water being omitted by enhancing the edge and detail information in

[1]Online. [Available]: http://gdex.cr.usgs.gov/gdex/

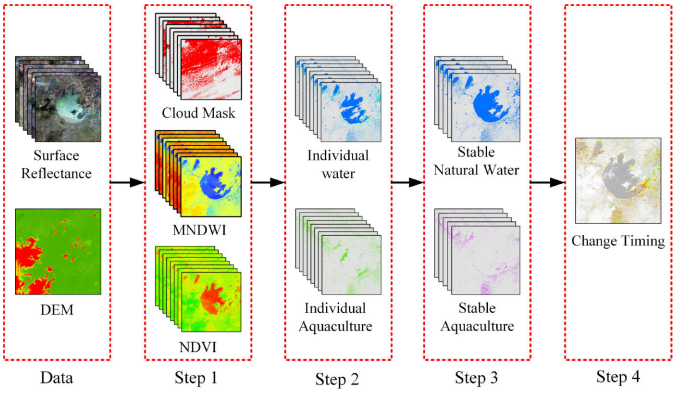

Fig. 4. Overview of delivery system.

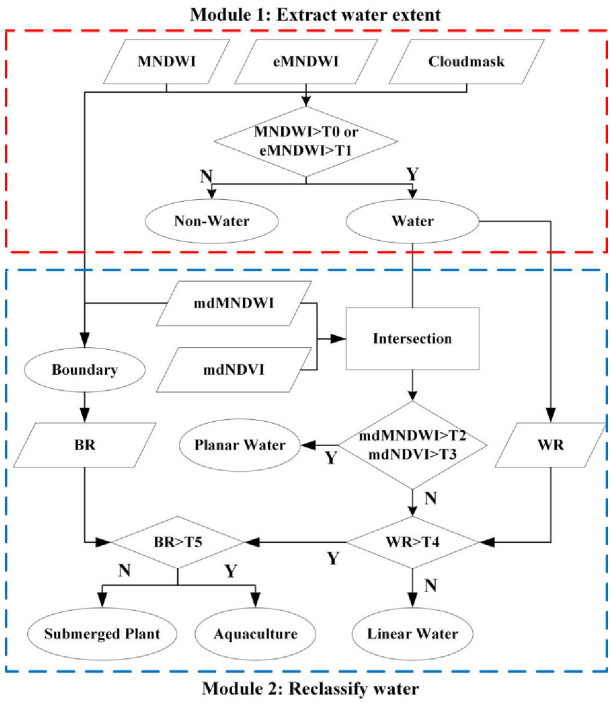

Fig. 5. Workflow of producing individual water map.

this study [41], the effectiveness of unsharp masking method was shown in Fig. 7. In the unsharp masking algorithm, the positive scaling factor that controls the level of contrast enhancement achieved at the output was calculated by subtracting the median-filtered MNDWI (mdMNDWI) from the MNDWI image, and the enhanced MNDWI image (eMNDWI) is obtained from the MNDWI as

$$\text{eMNDWI} = \text{MNDWI} + (\text{MNDWI} - \text{mdMNDWI}). \quad (3)$$

Suitable thresholds for water extracting varied within a year for the physical properties of water changes, and a fixed threshold may cause oversegmentation or undersegmentation, so OTSU was used to find an adaptive threshold to identify the water mask from the background in this study [42].The workflow extracting water mask is shown in Module 1 of Fig. 5.

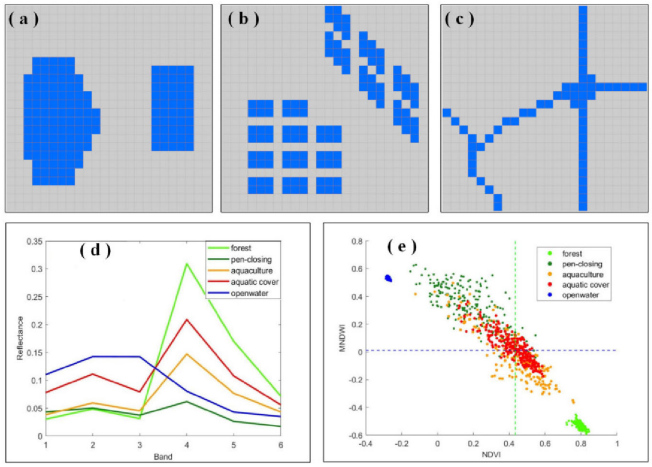

Fig. 6. Typical water types and their spectral characteristics in the study area. (a) Structural model of planar water. (b) Structural model of aquaculture water. (c) Structural model of linear water. (d) Spectral curves for representative ground targets (Landsat form). (e) Scatter plots of NDVI versus MNDWI, and the green dotted line indicates the mean value of NDVI of the whole study area.

B. Individual Water Map

Based on the water body mask extracted earlier, a decision tree method was used to distinguish surface water into natural water and aquaculture. The geofeatures of aquaculture could be described as aquatic plant-intensive, planar water, divided into grids by artificial boundaries, and these three features were used to distinguish aquaculture from deep water, rivers, and natural wetlands. As shown in Module 2 of Fig. 5, a decision tree was designed to extract aquaculture land. Deep water was easily identified using MNDWI and NDVI, whereas changes in aquatic plant phenology and water level make that aquaculture, narrow rivers, and natural wetlands have similar spectral information (see Fig. 6), and it was difficult to identify aquaculture only use these two indices. Fortunately, the unique texture of aquaculture makes it distinguishable, as shown in Fig. 6.

The local mean filtering with 5×5 windows is an effective texture feature to estimate the water ratio (WR) and the boundary ratio (BR) of aquaculture. WR is the local mean of water mask in this method, and aquaculture had a WR value larger than narrow rivers. BR is the local mean of boundary mask, and aquaculture had a WR value larger than natural wetlands. The boundary mask marks the artificial boundary inside the aquaculture base, and was calculated by the (3) in this article

$$\text{Boundary} = (\text{MNDWI} - \text{mdMNDWI}) < -0.1. \quad (4)$$

Several thresholds were used in this method, where T3 is the mean value of mdNDVI, and the other thresholds, including T0, T1, T2, T4, and T5, are adaptive thresholds obtained by the OTSU method.

C. Frequency-Based Method for Extracting Stable Water

The cloud coverage problems were inevitable in the Taihu Lake Basin. Most image scenes were partially or completely covered by cloud, resulting in that only about 40% observations

were available in each year. The uncertainty caused by the changes in aquatic plant phenology and water level was another problem [36]. In addition, emergencies, such as precipitation or irrigation, could also cause some error. These issues make it difficult to obtain accurate water from an image or a composite image.

A frequency-based method of time series was used to extract stable water body and removes the targets causing commission or omission error. Those targets will be processed in a different way according to their frequency of occurrence in a year. Low-frequency targets, such as moist land after rain, seasonal snowfall, and ponds with low water levels, were filtered out by the frequency-based approach. High-frequency targets, such as cloud coverage and mountain shadows are the main cause of the wrong identification of water body, were masked out in previous work. All images of single–temporal water and cloud in each year are accumulated and (5) is used to calculate the annual frequency of surface water

$$F_w = \frac{N_w}{N_a - N_m} \tag{5}$$

where F_w is the frequency of surface water, N_w is the accumulative number of observed water, N_a is the number of all binary water maps, and N_m is the number of the observed cloud. Then, annual stable water pixels with high occurrence frequency were segmented by the OTSU method.

D. Spatial–Temporal Change Detection

In order to detect the temporal and spatial changes of the surface water body in the Taihu Lake region, the postclassification cross-tabulation technique was chosen to extract the location of water changes each year. Classification results for each adjacent two years were compared and the change was detected from the overlaid data. There were six main types of water disturbance in the past 35 years, which are natural water to nonwater, nonwater to natural water, nonwater to aquaculture, aquaculture to nonwater, natural water to aquaculture, and aquaculture to natural water. Each type of transitions was saved in a timing raster, which gives breakpoint timing values in decimal year format. The quantitative characteristics of water disturbance in Taihu Lake area were also analyzed.

E. Validation

Two validation datasets were used to evaluate the performance of the classification system in this article, the first is the higher resolution classification image obtained by the visual interpretation of Sentinel-2 images, and the second is to generate space-time samples from the study area using TimeSync+ application.

Sentinel-2 images, with superior high spatial and radiometric resolution, are ideal data for identifying surface water body. Some narrow waterway and small water are omitted by Landsat images (smaller than a Landsat pixel resolution), which can be very accurately identified in Sentinel images. Three Sentinel-2 images of 2015 (acquired on August 28, 2015, December 16, 2015, and December 26, 2015) and GDEM data were imported into an expert knowledge system and assisted by artificial visual interpretation to produce reference data, and a 10-m resolution water cover map was produced as the ground truth data. The confusion matrix was calculated to evaluate the accuracy of the results.

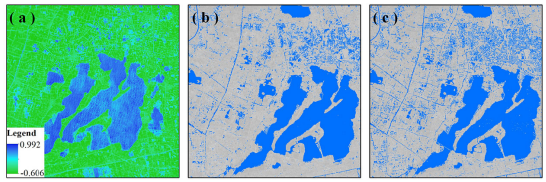

Fig. 7. Effectiveness of unsharp masking method in extracting water mask. (a) MNDWI image of a small block of the study area. (b) Water mask extracted from MNDWI image. (c) Water mask extracted from eMNDWI image.

TimeSync+ is an application for gathering point and polygon spectral–temporal information from Landsat time series data into a database, commonly used for spatial–temporal change verification [43]. The operating process is given as follows in this article.

First, 460 sampling sites were generated in the study area, including 400 random sampling sites, and 60 field sampling sites that were used to determine the surface features, the distribution of the sampling sites is shown Fig. 8. Second, spatial–temporal samples from 1985 to 2019 in the study area were collected using the TimeSync+ plug-in, and the median composite images from June to September each year were generated and preserved in tile image formats. During the sample marking stage, each sample was marked as nonwater, natural water, or aquaculture, and the segments of spectral trajectory were marked as stable nonwater, stable natural water, stable aquaculture, emerging water, land from water, emerging aquaculture, land from aquaculture, water used as aquaculture, or water recovered from aquaculture. Among them, 15 sampling sites were deleted because they were difficult to be identified or contained too many mixed pixels, and the 15 575 samples of 445 sampling sites were retained. Next, the pixel value on the classification image at the corresponding sampling sites was obtained and added to the validation dataset. Finally, this validation dataset is used to evaluate the overall performance of the classification and confusion matrix was calculated.

IV. Results and Discussions

A. Stable Water Extraction and Mapping

Fig. 9 shows the ground truth and several classification results of this study. Three 10-m multispectral Sentinel-2 images [see Fig. 9(a)] were used to generate the accurate stable water map of 2015 [see Fig. 9(b)]. Moreover the map was used to verify the accuracy of GSW [see Fig. 9(c)] and the confusion matrix, as shown in Table I. The accuracy was calculated in this study [see Fig. 9(d)], with OA = 95.33%, kappa = 0.8903, of which the PA and UA of the water reached 91.14% and 93.69%, respectively. The source of error in our method is mainly derived from the resolution limit of the image, and some of the trails between fish ponds are classified into the water body, which makes the area of the fish pond dense area overvalued. But the accuracy of our product is better than that of GSW, and shallow water body,

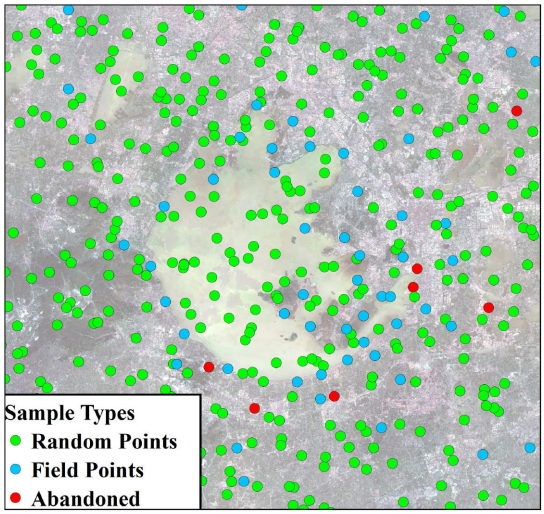

Fig. 8. Location of sample sites.

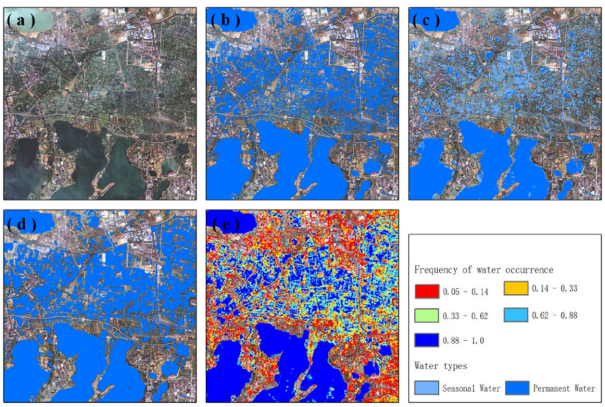

Fig. 9. Ground truth and several classification results. (a) True color composite image of the Sentinel-2. (b) Interpretation results of surface water on 10-m resolution Sentinel-2 image. (c) Water mask from GSW. (d) 30-m water map of Landsat in this study. (e) Water frequency calculated in this study. (f) Legends.

TABLE I
CONFUSION MATRIX OF WATER EXTENT SHOWN AS SAMPLE COUNTS

		Reference			
		Water	Non-water	Total	UA(%)
Map	Water	3589520	241806	3831326	93.69
	Non-water	349030	8483244	8832274	96.05
	Total	3938500	8725050	12663600	
	PA(%)	91.14	97.23		
OA=95.33%, kappa=0.8903					

which was omitted in GSW products, rivers, and aquaculture bases with high occurrence frequency [see Fig. 9(e)], was well extracted in this study, and the rivers show more continuous and the lakes more complete.

As shown in Table II, the classifications of surface water have high accuracies, with OAs of 95.83% and kappa of 0.894. Both the UA and PA of nonwater are greater than 98%, indicating that the classification system performs well in distinguishing water from nonwater in this article. The PA (92.85%) and UA (91.48%) of natural water are lower than nonwater, whereas the PA (72.35%) and UA (72.79%) in aquaculture are lowest, and the confusion matrix indicates that some samples have been mixed between natural water bodies and aquaculture, which is the main source of error in this article.

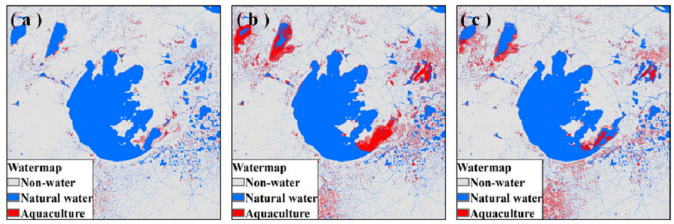

Fig. 10. Yearly stable water map in Taihu Lake area. (a) Water map of 1985. (b) Water map of 2003. (c) Water map of 2018.

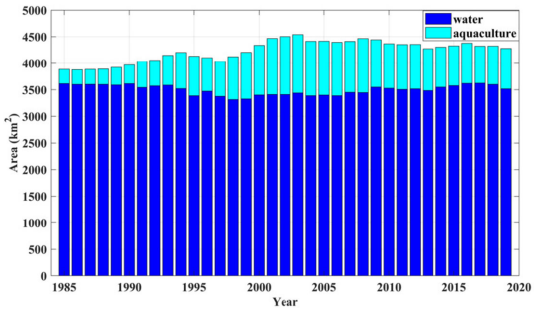

Fig. 11. Annual area statistics of surface water in Taihu Lake.

B. Annual Distribution of Water

The total water area of the study area in 1985 was 3885.6 km^2, and the area of the natural water was about 93.0%, up to 3614.7 km^2, whereas the aquaculture water is about 7.0%, up to 270.9 km^2 [see Fig. 10(a)]. The largest surface water cover around Taihu Lake was in 2003 with the total area increasing to 4539.1 km^2, and the area of aquaculture water grew 24.2%, up to 1099.6 km^2, whereas the area of the natural water reduced to 75.8%, down to 3439.5 km^2 [see Fig. 10(b)]. The latest total water area (in 2018) increased to 4321.5 km^2, and the area of the natural water reincreased to 83.3%, up to 3599.7 km^2, whereas the area of aquaculture water decreased to 16.7%, down to 721.8 km^2 [see Fig. 10(c)].

As shown in Fig. 11, during 1985–2003, although the area of natural water bodies continued to decrease (-9.74 km^2/a), the area of aquaculture water bodies increased rapidly (46.04 km^2/a), resulting in an increasing trend of a total surface water body area (36.3 km^2/a). After 2003, natural water bodies continued to increase (10.68 km^2/a), whereas the area of aquaculture water bodies decreased rapidly (-25.19 km^2/a), and the total surface water showed a downward trend (-14.5 km^2/a). Over the past 35 years, the change of aquaculture water is the main reason for the change in the total area of the surface water around Taihu Lake.

TABLE II
CONFUSION MATRIX OF WATER MAPPING SHOWN AS SAMPLE COUNTS

		Reference				
		Non-water	Natural-water	Aquaculture	Total	UA(%)
Map	Non-water	11531	110	55	11696	98.59
	Natural-water	85	2792	175	3052	91.48
	Aquaculture	120	105	602	827	72.79
	Total	11736	3007	832	15575	
	PA(%)	98.25	92.85	72.35		
OA=95.83%, kappa=0.894						

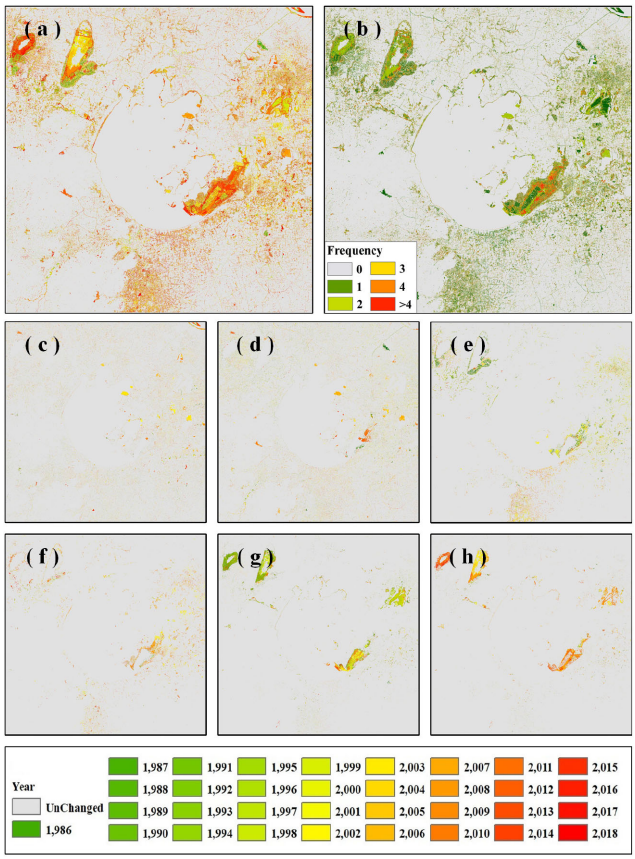

Fig. 12. Timing raster of surface water change in Taihu Lake during 1984–2018. (a) Timing raster of water-type changes. (b) Frequency of changes. (c) Timing raster of natural water converted into nonwater. (d) Timing raster of nonwater converted into natural water. (e) Timing raster of nonwater converted into aquaculture water. (f) Timing raster of aquaculture water converted into nonwater. (g) Timing raster of natural water used as aquaculture water. (h) Timing raster of natural water recovered from aquaculture water.

C. Temporal and Spatial Changes of Surface Water

In order to further explore on how the surface water changes, a spatial–temporal analysis of surface water around Taihu Lake carried out based on the annual water map and a change timing raster is calculated, as showed in Fig. 12(a). The changes in surface water bodies occurred mainly in the northwest corner of the study area near Ge Lake and ChangDang Lake, most area of Suzhou, the East Taihu area, and Donglin Town in Huzhou. The changes lasted from 1986 to 2018. In some regions, several surface water change events have been occurred for several times, especially more than four times changes have occurred in parts of East Taihu Lake, as shown in Fig. 12(b).

The types of changes in surface water include the change from nonwater to natural water (new water), natural water to nonwater (lost water), nonwater to aquaculture (new aqua), aquaculture to nonwater (lost aqua), natural water to aquaculture (water-aqua), and aquaculture to natural water (aqua-water). The timing raster of each type of change was generated and displayed in Fig. 12.

Fig. 12(c) shows the time and location of changes that natural water was converted into nonwater. The leading causes of this type of change are the shrinking of rivers and lakes affected by climate change and human-made land reclamation. Among them, the reclamation events mainly occurred at some lake areas in Suzhou City from 2002 to 2004. Fig. 12(d) is the timing raster of transformation from nonwater to natural water. The main causes of this type of change are the expansion of rivers and lakes affected by climate change, water recovered from land reclamation, and artificially excavated of reservoirs and rivers with the support of water conservation projects. Among them, the events of water recovering from reclamation mainly occurred in Suzhou City in 2008. Almost aquabreeding water was recovered into natural water. After 2008, several reservoirs and rivers were excavated in the mountains to the southwest of Taihu Lake. During 2013–2014, a large piece of land in East Taihu Lake was transformed into water under the guidance of policy.

Fig. 12(e) shows the time and location of changes from nonwater to aquaculture. Due to the high demand for water, the emerging aquaculture bases are mainly located in flat and water-rich areas, such as the area around Ge Lake and ChangDang Lake, the land near East Taihu Lake, the plains to the north of Yangcheng Lake, and the plains surrounding the DongTiao River in the southern part of Huzhou City. The area of new emerging aquaculture bases has increased continuously from 1986 to 2018, and the speed reached the top during 1999–2000. Fig. 12(f) shows the time and location of changes from aquaculture to nonwater. Urban expansion and restoration of farmland are the main reasons for the disappearance of aquaculture water bodies, especially during 2000–2005. The construction area of Suzhou City and Huzhou City continued to expand, resulting in more than 40-km^2 aquaculture land converting into construction land.

Fig. 12(g) is the timing raster of natural water used as aquaculture water. This kind of change mainly occurs in great lakes. Aquaculture started to appear in Ge Lake and ChangDang Lake in 1993, developed rapidly from 1995 to 2003. In 2003,

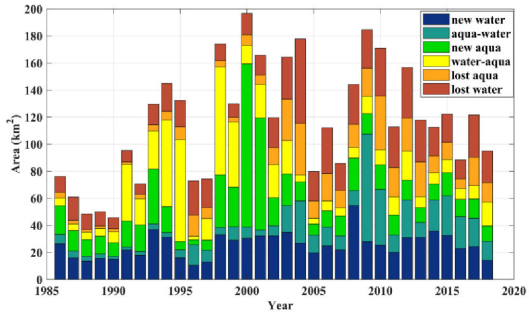

Fig. 13. Statistics on the types and areas of surface water disturbances from 1986 to 2018.

aquaculture covered most of the waters of Ge Lake, ChangDang Lake, East Taihu Lake, and Yangcheng Lake, with the area reaching 370.5 km^2. After 2003, few other water bodies have been developed as aquaculture water. Fig. 12(h) shows the time and location of that aquaculture recovered as natural water. This type of change began at Ge Lake in 2003 and this change gradually occurs throughout the Taihu region from then on, with a number of aquaculture restored to natural water. All aquaculture at Ge Lake has been recovered into the natural water from 2003 to 2009 under the guidance of Ecological Restoration Project of Ge Lake (2003). During 2009 to 2018, a large amount of aquaculture in ChangDang Lake, Yangcheng Lake, and East Taihu Lake were restored to water, especially, all aquaculture in ChangDang Lake have been restored to natural water, driven by a series of policies, such as East Taihu Comprehensive Rehabilitation Project (2008 and 2013). From 2003 to 2018, a total area of 274 km^2 of aquaculture was restored to natural water, accounting for approximately 74% of the most significant areas of farmed water in the past 35 years.

In general, as shown in Fig. 13, the changes of the water body in the study area are mainly divided into two stages, the area of the whole surface water showed an increasing trend before 2003, whereas a decreasing trend after 2003. The emergence and disappearance of aquaculture water are the main disturbance, and the reclamation and restoration of natural water are also an important disturbance. Although the effects of interannual fluctuations in climate cannot be ignored, they are much smaller than those of human activities.

In addition, it should be noted that the conversion between natural and aquaculture waters has been a very significant water disturbance since 1993. A very large number of aquaculture appeared in several large lakes, which poses a significant threat to water quality and water safety in the area around Taihu Lake.

Policy interventions had a significant impact on water disturbances around Taihu Lake. A total area of 714.5 km^2 of aquaculture water converted into other land use during 2003–2018, of which the policy-directed water recover from aquaculture is about 380 km^2 and accounts for 53% of the total reduction.

V. Conclusion

This study demonstrates annual water distribution and human-induced spatial–temporal water disturbance in Taihu Lake region over the past 35 years by using time series Landsat images. This research conducts from two points. First, the omission of narrow river and lake boundaries could be avoided when the details of the water index images were enhanced by an unsharp masking method. Second, texture features are more helpful than spectral and phenological features for distinguishing aquaculture from natural water, which makes that the proposed method has a better performance than previous studies in water extraction and aquaculture identification.

Human activity has played a very important role in the water disturbance around Taihu Lake during last 35 years. Aquaculture water showed a trend of rapid increase while natural water showed a trend of slow decrease due to the development of aquaculture and reclamation, and the share of aquaculture in total water reached the peak in 2003 (about 24.2%), then both aquaculture and natural water showed the reverse trend because of a series of ecological restoration and water conservancy projects adopted in this area.

Future work will involve improving the accuracy of small-scale aquaculture identification (less than 10 pixels) to overcome the problem of undervaluation of aquaculture. Nevertheless, the proposed method can effectively monitor human-induced water disturbance and progress in the implementation of ecological and water conservancy projects, it is greatly helpful for water management and water safety.

References

[1] A. P. Shevyrnogov, A. V. Kartushinsky, and G. S. Vysotskaya, "Application of satellite data for investigation of dynamic processes in inland water bodies: Lake Shira (Khakasia, Siberia), a case study," *Aquatic Ecol.*, vol. 36, no. 2, pp. 153–163, 2002.

[2] J. S. Famiglietti and M. Rodell, "Water in the balance," *Sci.*, vol. 340, no. 6138, pp. 1300–1301, 2013. [Online]. Available: http://science.sciencemag.org/content/340/6138/1300.abstract

[3] C. Zhang, C. Zhao, A. Zhou, K. Zhang, R. Wang, and J. Shen, "Late Holocene lacustrine environmental and ecological changes caused by anthropogenic activities in the Chinese Loess Plateau," *Quaternary Sci. Rev.*, vol. 203, pp. 266–277, 2019. [Online]. Available: http://www.sciencedirect.com/science/article/pii/S0277379118302622

[4] R. Tateishi *et al.*, "Production of global land cover data—GLCNMO," *Int. J. Digit. Earth*, vol. 4, no. 1, pp. 22–49, 2011. [Online]. Available: https://doi.org/10.1080/17538941003777521

[5] G. Gutman, C. Huang, G. Chander, P. Noojipady, and J. G. Masek, "Assessment of the NASA-USGS Global Land Survey (GLS) datasets," *Remote Sens. Environ.*, vol. 134, pp. 249–265, 2013.

[6] J. Chen *et al.*, "Global land cover mapping at 30 m resolution: A POK-based operational approach," *ISPRS J. Photogrammetry Remote Sens.*, vol. 103, pp. 7–27, 2015. [Online]. Available: http://www.sciencedirect.com/science/article/pii/S0924271614002275

[7] Y. K. Yang, P. F. Xiao, X. Z. Feng, and H. X. Li, "Accuracy assessment of seven global land cover datasets over China," *ISPRS J. Photogrammetry Remote Sens.*, vol. 125, pp. 156–173, 2017.

[8] P. Gong *et al.*, "Stable classification with limited sample: Transferring a 30-m resolution sample set collected in 2015 to mapping 10-m resolution global land cover in 2017," *Sci. Bull.*, 2019. [Online]. Available: http://www.sciencedirect.com/science/article/pii/S2095927319301380

[9] J. Nowosad, T. F. Stepinski, and P. Netzel, "Global assessment and mapping of changes in mesoscale landscapes: 1992–2015," *Int. J. Appl. Earth Observ. Geoinf.*, vol. 78, pp. 332–340, 2019. [Online]. Available: http://www.sciencedirect.com/science/article/pii/S0303243418305841

[10] M. L. Carroll, J. R. Townshend, C. M. DiMiceli, P. Noojipady, and R. A. Sohlberg, "A new global raster water mask at 250 m resolution," *Int. J. Digit. Earth*, vol. 2, no. 4, pp. 291–308, 2009.

[11] C. Verpoorter, T. Kutser, D. A. Seekell, and L. J. Tranvik, "A global inventory of lakes based on high-resolution satellite imagery," *Geophys. Res. Lett.*, vol. 41, no. 18, pp. 6396–6402, 2014.

[12] E. Fluet-Chouinard, B. Lehner, L.-M. Rebelo, F. Papa, and S. K. Hamilton, "Development of a global inundation map at high spatial resolution from topographic downscaling of coarse-scale remote sensing data," *Remote Sens. Environ.*, vol. 158, pp. 348–361, 2015.

[13] D. Yamazaki, M. A. Trigg, and D. Ikeshima, "Development of a global 90 m water body map using multi-temporal Landsat images," *Remote Sens. Environ.*, vol. 171, pp. 337–351, 2015. [Online]. Available: http://www.sciencedirect.com/science/article/pii/S0034425715301656
[14] M. Feng, J. O. Sexton, S. Channan, and J. R. Townshend, "A global, high-resolution (30-m) inland water body dataset for 2000: First results of a topographic–spectral classification algorithm," *Int. J. Digit. Earth*, vol. 9, no. 2, pp. 113–133, 2016. [Online]. Available: https://doi.org/10.1080/17538947.2015.1026420
[15] J.-F. Pekel, A. Cottam, N. Gorelick, and A. S. Belward, "High-resolution mapping of global surface water and its long-term changes," *Nature*, vol. 540, no. 7633, pp. 418–422, 2016.
[16] I. Klein, U. Gessner, A. J. Dietz, and C. Kuenzer, "Global waterpack—A 250 m resolution dataset revealing the daily dynamics of global inland water bodies," *Remote Sens. Environ.*, vol. 198, pp. 345–362, 2017.
[17] M. Pal, "Random forest classifier for remote sensing classification," *Int. J. Remote Sens.*, vol. 26, no. 1, pp. 217–222, 2005.
[18] M. Pal and P. M. Mather, "Support vector machines for classification in remote sensing," *Int. J. Remote Sens.*, vol. 26, no. 5, pp. 1007–1011, 2005.
[19] G. Mountrakis, J. Im, and C. Ogole, "Support vector machines in remote sensing: A review," *ISPRS J. Photogrammetry Remote Sens.*, vol. 66, no. 3, pp. 247–259, 2011.
[20] M. Fernandez-Delgado, E. Cernadas, S. Barro, and D. Amorim, "Do we need hundreds of classifiers to solve real world classification problems?" *J. Mach. Learn. Res.*, vol. 15, pp. 3133–3181, 2014.
[21] M. Belgiu and L. Dragut, "Random forest in remote sensing: A review of applications and future directions," *ISPRS J. Photogrammetry Remote Sens.*, vol. 114, pp. 24–31, 2016.
[22] K. Singh, M. Ghosh, and S. R. Sharma, "WSB-DA: Water surface boundary detection algorithm using Landsat 8 OLI data," *IEEE J. Sel. Topics Appl. Earth Observ. Remote Sens.*, vol. 9, no. 1, pp. 363–368, Jan. 2016.
[23] E. P. Crist, "A TM tasseled cap equivalent transformation for reflectance factor data," *Remote Sens. Environ.*, vol. 17, no. 3, pp. 301–306, 1985. [Online]. Available: http://www.sciencedirect.com/science/article/pii/0034425785901026
[24] S. K. McFeeters, "The use of the normalized difference water Index in the delineation of open water features," *Int. J. Remote Sens.*, vol. 17, no. 7, pp. 1425–1432, 1996.
[25] H. Xu, "Modification of normalised difference water index (NDWI) to enhance open water features in remotely sensed imagery," *Int. J. Remote Sens.*, vol. 27, no. 14, pp. 3025–3033, 2006.
[26] G. L. Feyisa, H. Meilby, R. Fensholt, and S. R. Proud, "Automated water extraction index: A new technique for surface water mapping using Landsat imagery," *Remote Sens. Environ.*, vol. 140, pp. 23–35, 2014. [Online]. Available: http://www.sciencedirect.com/science/article/pii/S0034425713002873
[27] A. Fisher, N. Flood, and T. Danaher, "Comparing Landsat water index methods for automated water classification in eastern Australia," *Remote Sens. Environ.*, vol. 175, pp. 167–182, 2016. [Online]. Available: http://www.sciencedirect.com/science/article/pii/S0034425715302753
[28] C. Huang, Y. Chen, and J. Wu, "Mapping spatio-temporal flood inundation dynamics at large river basin scale using time-series flow data and MODIS imagery," *Int. J. Appl. Earth Observ. Geoinf.*, vol. 26, pp. 350–362, 2014.
[29] C. Huang, Y. Chen, S. Zhang, and J. Wu, "Detecting, extracting, and monitoring surface water from space using optical sensors: A review," *Rev. Geophys.*, vol. 56, no. 2, pp. 333–360, 2018.
[30] H. Jiang, M. Feng, Y. Zhu, N. Lu, J. Huang, and T. Xiao, "An automated method for extracting rivers and lakes from Landsat imagery," *Remote Sens.*, vol. 6, no. 6, pp. 5067–5089, 2014.
[31] Y. Yang *et al.*, "Landsat 8 OLI image based terrestrial water extraction from heterogeneous backgrounds using a reflectance homogenization approach," *Remote Sens. Environ.*, vol. 171, pp. 14–32, 2015.
[32] C. Huang, N. Ba Duy, S. Zhang, S. Cao, and W. Wagner, "A comparison of terrain indices toward their ability in assisting surface water mapping from Sentinel-1 data," *ISPRS Int. J. Geo-Inf.*, vol. 6, no. 5, 2017, Art. no. 140.
[33] T. Zhang, Q. Li, X. Yang, C. Zhou, and F. Su, "Automatic mapping aquaculture in coastal zone from TM imagery with OBIA approach," in *Proc. 18th Int. Conf. Geoinf.*, 2010, pp. 1–4.
[34] Z. Zeng, D. Wang, W. Tan, and J. Huang, "Extracting aquaculture ponds from natural water surfaces around inland lakes on medium resolution multispectral images," *Int. J. Appl. Earth Observ. Geoinf.*, vol. 80, pp. 13–25, 2019. [Online]. Available: http://www.sciencedirect.com/science/article/pii/S0303243418309620
[35] S. L. Ozesmi and M. E. Bauer, "Satellite remote sensing of wetlands," *Wetlands Ecol. Manage.*, vol. 10, no. 5, pp. 381–402, 2002.
[36] M. Borro, N. Morandeira, M. Salvia, P. Minotti, P. Perna, and P. Kandus, "Mapping shallow lakes in a large South American floodplain: A frequency approach on multitemporal Landsat TM/ETM data," *J. Hydrol.*, vol. 512, pp. 39–52, 2014.
[37] X. Wang *et al.*, "Tracking annual changes of coastal tidal flats in China during 1986–2016 through analyses of Landsat images with Google Earth Engine," *Remote Sens. Environ.*, 2018. [Online]. Available: http://www.sciencedirect.com/science/article/pii/S003442571830539X
[38] Z. Zhu and C. E. Woodcock, "Continuous change detection and classification of land cover using all available Landsat data," *Remote Sens. Environ.*, vol. 144, pp. 152–171, 2014. [Online]. Available: http://www.sciencedirect.com/science/article/pii/S0034425714000248
[39] E. Hamunyela, J. Verbesselt, and M. Herold, "Using spatial context to improve early detection of deforestation from Landsat time series," *Remote Sens. Environ.*, vol. 172, pp. 126–138, 2016. [Online]. Available: http://www.sciencedirect.com/science/article/pii/S0034425715301942
[40] Z. Zhu and C. E. Woodcock, "Object-based cloud and cloud shadow detection in Landsat imagery," *Remote Sens. Environ.*, vol. 118, pp. 83–94, 2012. [Online]. Available: http://www.sciencedirect.com/science/article/pii/S0034425711003853
[41] A. Polesel, G. Ramponi, and V. J. Mathews, "Image enhancement via adaptive unsharp masking," *IEEE Trans. Image Process.*, vol. 9, no. 3, pp. 505–510, Mar. 2000.
[42] N. Otsu, "A threshold selection method from gray-level histograms," *IEEE Trans. Syst., Man, Cybern.*, vol. SMC-9, no. 1, pp. 62–66, Jan. 1979.
[43] W. B. Cohen, Z. Yang, and R. Kennedy, "Detecting trends in forest disturbance and recovery using yearly Landsat time series: 2. TimeSync—Tools for calibration and validation," *Remote Sens. Environ.*, vol. 114, no. 12, pp. 2911–2924, 2010. [Online]. Available: http://www.sciencedirect.com/science/article/pii/S0034425710002269

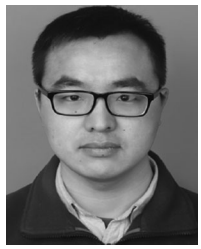

Yaping Meng received the B.S. degree in geographic and oceanographic sciences, in 2014 from Nanjing University, Nanjing, China, where he is currently working toward the Ph.D. degree with Jiangsu Provincial Key Laboratory of Geographic Information Science and Technology.

His research interests include image processing, time series image analysis, and climate change.

Peijun Du (Senior Member, IEEE) received the Ph.D. degree in geodesy and survey engineering from the China University of Mining and Technology, Xuzhou, China, in 2001.

He is currently a Professor of Remote Sensing and Geographical Information Science at Nanjing University, Nanjing, China. He has authored or coauthored more than 70 articles in international peer-reviewed journals, and more than 100 papers in international conferences, and Chinese journals. His research interests include remote sensing image processing and pattern recognition, hyperspectral remote sensing, and applications of geospatial information technologies.

Dr. Du is an Associate Editor for the IEEE GEOSCIENCE AND REMOTE SENSING LETTERS. He also served as the Co-Chair of the Technical Committee of URBAN2009, IAPR-PRRS 2012, EORSA2014, IEOAs 2015, and CCGC2015, the Co-Chair of the Local Organizing Committee of JURSE 2009, WHISPERS 2012, and EORSA 2012, and the member of Scientific Committee or Technical Committee of other international conferences, including WHISPERS (2010–2016), URBAN (2011, 2013, and 2015), MultiTemp (2011, 2013, and 2015), ISIDF 2011, and SPIE European Conference on Image and Signal Processing for Remote Sensing (2012–2016).

Xin Wang received the B.S. degree in geographic information system from Lanzhou University, Lanzhou, China, in 2016. He is currently working toward the Ph.D. degree in cartography and geographic information system with Nanjing University, Nanjing, China.

He is currently a Visiting Student with the Department of Geography and Planning, Queen's University, Kingston, ON, Canada. His research interests include multitemporal image processing, change detection, signal processing, and pattern recognition.

Xuyu Bai received the B.S. degree in resource environment and urban planning management from Beijing Normal University, Zhuhai, China, in 2013, and the M.A. degree in environmental management and consultancy from Lancaster University, Lancaster, U.K., in 2015. Since 2017, he has been working toward the Ph.D. degree in environment and resource remote sensing with Nanjing University, Nanjing, China.

He is currently a Visiting Researcher with Lancaster University. His research interests include environment assessment, environment remote sensing, and urban remote sensing.

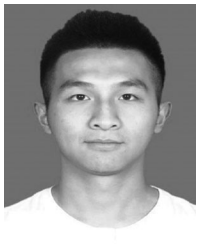

Shanchuan Guo received the M.S. degree in land resource management from the China University of Mining and Technology, Xuzhou, China, in 2018. He is currently working toward the Ph.D. degree with the School of Geography and Ocean Science, Nanjing University, Nanjing, China.

His research interests mainly include soil moisture retrieval, surface deformation monitoring from microwave remote sensing, and time series analysis.